

Article

Synergistic Effect of WS₂ and Micro-Textures to Inhibit Graphitization and Delamination of Micro-Nano Diamond-Coated Tools

Zhao Zhang ^{1,*}, Xudong Qin ¹, Silu Ma ¹, Yang Liu ², Liping Wang ¹ and Xinyang Zhao ¹¹ College of Electromechanical and Automotive Engineering, Yantai University, Yantai 264005, China² Jiaodong Quality Inspection Center, Yantai 264003, China

* Correspondence: trojanz@yeah.net

Abstract: Diamond-coated tools often fail due to coating graphitization and delamination caused by poor coating adhesion, large contact stress, and thermochemical reactions. To address these issues, this research utilized a combination of micro-nano double-layer diamond coating, WS₂ coating, and micro-textures. The WS₂ coating inhibits the graphitization of the diamond coating through a transfer film mechanism, while the micro-textures and nanocrystalline diamond coating store WS₂, resulting in a prolonged lubrication life. Additionally, the influence of micro-texture on coating-substrate residual stress and coating-substrate mechanical interlocking was discussed, and it was proved that proper micro-textures effectively improve the coating adhesion. Under the same cutting flux conditions, taking coating peeling as the judging standard, the cutting distance of textured WS₂/Micro-Nano diamond coating tool is more than three times that of ordinary, diamond-coated tools, which greatly improves the service life of the tool.

Keywords: microtextures; WS₂; Diamond-coated tools; coating adhesion; graphitization



Citation: Zhang, Z.; Qin, X.; Ma, S.; Liu, Y.; Wang, L.; Zhao, X. Synergistic Effect of WS₂ and Micro-Textures to Inhibit Graphitization and Delamination of Micro-Nano Diamond-Coated Tools. *Crystals* **2023**, *13*, 1034. <https://doi.org/10.3390/cryst13071034>

Academic Editors: Jiaqiang Dang, Yong Wang and Zongwei Ren

Received: 7 June 2023

Revised: 25 June 2023

Accepted: 26 June 2023

Published: 29 June 2023



Copyright: © 2023 by the authors. Licensee MDPI, Basel, Switzerland. This article is an open access article distributed under the terms and conditions of the Creative Commons Attribution (CC BY) license (<https://creativecommons.org/licenses/by/4.0/>).

1. Introduction

Diamond-coated tools have the advantage of high hardness, good wear resistance, low friction coefficient, and anti-stickiness, which are the best coated tools for processing high abrasive materials, such as graphite, carbon fiber, and high silicon aluminum alloy [1–3]. However, the graphitization of diamonds and the delamination of coating are noteworthy problems in the machining process. Especially in the machining of ferrous metals, the graphitization of diamonds is particularly serious [4]. Diamond is a metastable structure at room temperature; at high temperatures, carbon atoms separated from the tool surface can easily diffuse into the interstitial locations of the iron lattice, accelerating the wear of the coating [5]. Cutting heat and friction energy during the cutting process accelerated the conversion of diamond into graphite [6,7]. In addition, residual stress, coating-substrate interface defects, and external stress on the diamond coating are the main reasons for the delamination of the diamond coating [8,9]. Therefore, how to improve the anti-graphitization and anti-coating peeling ability of diamond-coated tools has become the focus of research in recent years.

Methods to inhibit graphitization of diamond tools are generally divided into ultrasonic-vibration-assisted cutting, liquid nitrogen cooling, low-temperature plasma-assisted cutting, surface nitriding treatment, tool lubrication, etc. [4,10,11]. Controlling the contact time of diamond and iron, reducing cutting temperature, and hindering the contact of tool-chip are the key thoughts of these methods. However, ultrasonic-assisted cutting brings repeated impact on the tool; crack initiation and expansion occur at the diamond-coating-substrate interface [12], which promotes the coating to peeling. The presence of lubricating fluid can form a lubricating film on the tool-chip-contacted surface. On the one hand, the heat generated by cutting is reduced, and on the other hand, the contact between the tool and

the workpiece is prevented, and the diffusion of elements is also suppressed. However, Chai [13] pointed out that the hydrodynamic pressure helps to introduce more liquid to the tip of the crack by means of squeezing, further enhancing the driving force of the crack tip. Consequently, liquid lubrication can inhibit the graphitization of diamonds-coated tools but increases the probability of diamond coating delamination. In this paper, the solid lubricant coating (SLC) was used to block the contact between C and Fe elements, decrease the cutting heat, and inhibit the graphitization of diamond coating. The application of SLC on cutting tools is widely studied, which significantly reduces cutting force and cutting temperature [14,15]. Excellent performance in reducing tool wear and is a very promising method for tool lubrication. The most commonly used solid lubricating coatings are WS_2 , MoS_2 , and graphite [16,17]. The good lubricity results from the layered structure of these soft coatings, which form transfer films under stress, and shear occurs between the middle layers of the coating [18]. An excellent synergy was formed by SLC and micro-textures. The solid lubricating coating has non-Amontonian frictional behavior and obtains a smaller coefficient of friction under the action of the micro-textures [19]. The composite effect of micro-textures and solid lubricating coating achieves good cutting performance on the tool [20,21].

Enhancing the coating adhesion, improving the quality of the diamond coating, and reducing the external stress and residual stress of the coating are the main methods to inhibit the delamination of the diamond coating [22–24]. In recent years, surface micro-textures have been used to improve the adhesion of the coating, and the mechanical interlocking phenomena between coating, base, and larger coating-base contact area are the main reasons for the increasing adhesion [25]. In addition, Meng et al. [26] consider that micro-textures were conducive to coatings in terms of wettability, phase composition, roughness and hardness, and specific surface area, which could enhance the interfacial properties of PVD coatings. This study exhibits innovation by applying solid lubricant coatings on diamond-coated cutting tools and synergizing with microtextures in the hopes of enhancing coating adhesion and reducing diamond graphitization. It avoids the negative effects of liquid nitrogen cooling zones and liquid lubricants on diamond-coated cutting tools, providing a fresh perspective for the development of such tools.

2. Experimental Details

The micro-texture of pits was processed by UV nanosecond laser at the position near the cutting edge in the front of the turning tool, as shown in Figure 1I, and the diameter of the micro-texture was about 30 μm . The tool material is cemented carbide YG6 (6% Co + 94% Co), which was etched by a high peak power ultraviolet nanosecond laser with a power >7W and 1.5 MHz repetition frequency. The surface of the sample was polished to remove the metal melt, which was produced by the laser shock wave, and the Co content of the surface was reduced with chemical reagents. The attack of the WC grains was performed using Murakami's solution (1.5 g $K_3Fe(CN)_6$ + 1.5 g KOH + 20 mL H_2O) for 15 min. In order to decrease the surface Co content, a wet chemical attack with an acid solution ($3H_2SO_4 + 7H_2O_2$) for 30 s. A total of 2 g diamond powder with a particle size of 5 μm was added to 30 mL acetone to form a suspension, and the tool was crystallized by an ultrasonic cleaner. Immersing the tool in the suspension for 15 min to implant diamond crystals ultrasonically. Subsequently, clean the turning tool with acetone for 5 min. Preparation of diamond coatings by Hot Wire Chemical Vapor Deposition (HFCVD, FHL600) as shown in Figure 1II. The tools were placed into the chamber, the temperature of the hot filament was regulated at 2200–2300 $^{\circ}\text{C}$, and the distance between the filament and the sample was 9 mm. Firstly, the microcrystalline diamond coating is grown on the turning tool, and then the nanocrystalline diamond coating is grown on top of the microcrystalline diamond coating. The specific experimental parameters are shown in Table 1.

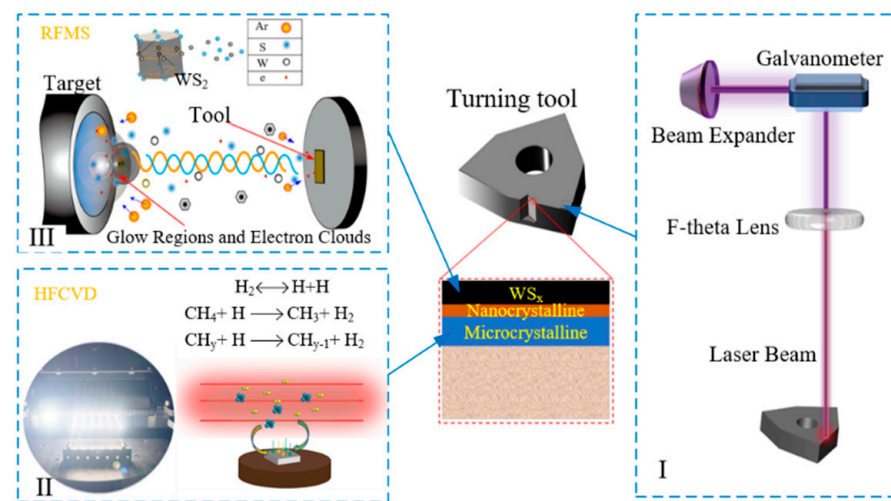


Figure 1. The preparation process of textured WS_2 /Diamond-coated tool. (I) The processing of microtextures (II) HFCVD (III) RFMS.

Table 1. The process parameters of the diamond coating.

Process Parameters	Microcrystalline		Nanocrystalline
	Nucleation Stage	Growth Stage	
Cavity pressure (Pa)	2500	1500	500
Filament temperature ($^{\circ}C$)	2250	2250	2250
CH_4 (sccm)	23.5	10.5	36
H_2 (sccm)	600	600	600
Deposition time (min)	60	240	90

In this research, the WS_2 coating was used to reduce the chip contact and inhibit the wear and graphitization of the diamond coating, but the adhesion between the diamond and WS_x was poor. In the experiment, the physical vapor deposition technology was used to prepare the W layer as the interlayer between the diamond and WS_2 . WC is formed between the W layer and diamond coating, resulting in a strong binding force [27]. Additionally, W and WS_2 form a metal bond, which greatly improves the diamond coating and soft coating. After the diamond coating was grown, the interlayer W was deposited on the tool by DC magnetron sputtering, and WS_2 was deposited on W by radio frequency magnetron sputtering (RFMS, MS-200), as shown in Figure 1III. W and WS_2 form a metal bond, which greatly improves the diamond coating and soft coating. The specific experimental parameters are shown in Table 2.

Table 2. The process parameters of WS_2 coating.

Process Parameters	WS_2	W
Cavity pressure (Pa)	1	0.8
Power (W)	110	72
Bias supply (V)	−70	−120
Ar (sccm)	28	28
Deposition time (min)	120	4
Power type	Radio frequency	Direct current

The microstructure is detected by SEM (Inspect S50). The displacement loading experiment utilizes a Rockwell indentation testing machine with a load of 1471N. The ultra-depth microscope can obtain pictures of different depths and stitch them into three-dimensional images. The Raman spectrometer is used to detect the crystal structure of C and

analyze the graphite phase in the diamond. A series of cutting experiments were performed on an S1-CA6140 lathe (Figure 2). Figure 1 and Table 1 show the experimental setup and experimental conditions, respectively. The bar was clamped on a lathe and machined with different turning tools, and the wear of the tools after cutting was observed. Cutting tests were carried out on the lathe using WS₂/Micro-Diamond Coating tool (W/MDCT), WS₂/micro-nano diamond coating tool (W/MNDCT), and textured WS₂/micro-nano diamond coating tool (T-W/MNDCT). All cutting tests were carried out under the same conditions (Table 3). The wear pattern of the tools and coating peeling were observed to judge the cutting performance of the tools.

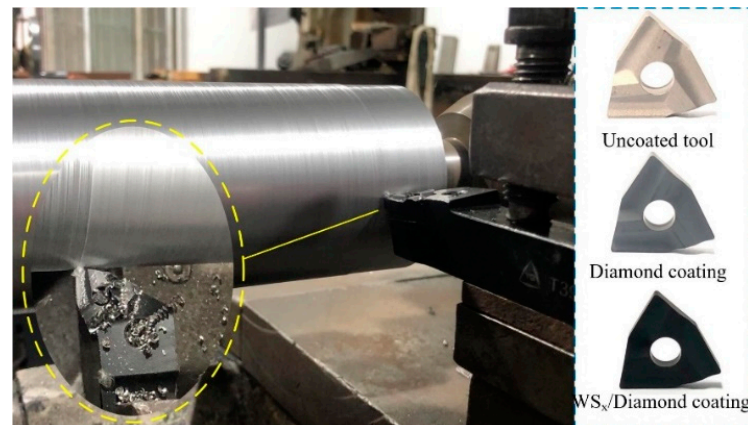


Figure 2. Cutting test on S1-CA6140 lathe.

Table 3. Cutting test conditions.

Machine Tool	S1-CA6140
Tool specifications	T31305F Maker: Zigong Great Wall
Tool material	YG6 (94% WC, 6% Co)
Bar material	45# (EN C45)
Rotational speed of bar	200 r/min
Depth of cut	0.3
Feed rate	0.12

3. Fundamental Research

3.1. Failure Forms of Diamond-Coated Tools

As the main failure mode of Diamond-coated tools, coating delamination is the core issue that must be addressed. The coating peeling area includes the cutting edge, rake face, and other parts with large force (Figure 3a). During the cutting process, the cutting position is subjected to a very large reaction force. The pyramid-shaped grains of the microcrystalline diamond could form a micro-cutting effect on the chips, and the large external stress (σ_e) could be generated accordingly (Figure 3b). The high temperature caused by the cutting heat is transferred to the coating-substrate interface, and the difference in the thermal expansion coefficient of the coating-substrate causes thermal stress (σ_t). Additionally, residual stress (σ_r) exists in the coating-substrate system during the preparation process (Figure 3c) [28]. The above-mentioned total stress (The sum of σ_e , σ_r , and σ_t) is greater than the interfacial bond strength (σ_f) could cause the coating to peel off, as shown in Equation (1).

$$\sigma_e + \sigma_r + \sigma_t > \sigma_f \quad (1)$$

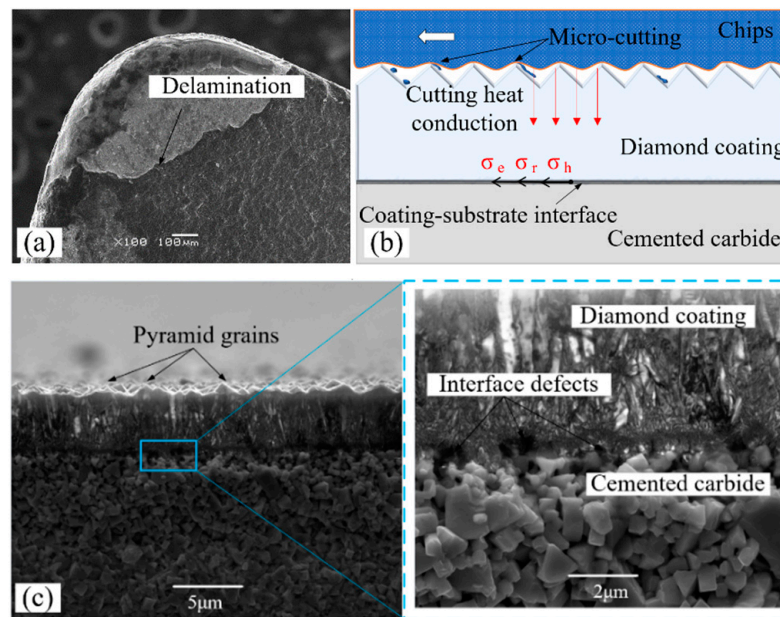


Figure 3. Analysis of delamination mechanism of diamond coatings. (a) The delamination of diamond coating (b) Stress analysis of coating-based systems (c) The cross-section of coating-substrate systems.

Wear is another failure model for diamond-coated tools. Especially in cutting ferrous metals, the high temperature, large stress, and catalytic action of ferrous metals accelerate the wear of diamond coatings [29]. Plowing wear of the diamond coating on the front cutter surface was found after machining the ferrous metal (Figure 4a). As an ultrahard material, the appearance of plow scratches on the surface of diamond coating show that chemical wear occurs. The Raman spectroscopy provides a fast, non-destructive means of characterizing carbon materials. The single sharp peak at 1332 cm^{-1} corresponds to the vibration of the sp^3 diamond lattice. The G peak ($1500\text{--}1580\text{ cm}^{-1}$) represents disordered carbon [30]. Compared with the unworn diamond coating, the range of the G peak is significantly increased, and the intensity of the D peak is decreased, indicating that the diamond coating has undergone graphitization during the wear process. Additionally, furrows appeared on the worn surface, indicating that the diamond coating was transformed into softer graphite. Based on the above analysis, the fundamental reason for the wear of Diamond-coated tools is the graphitization of diamonds. The high temperature, large stress, and the reaction of diamond and iron at high temperatures during cutting play an important role in the graphitization process.

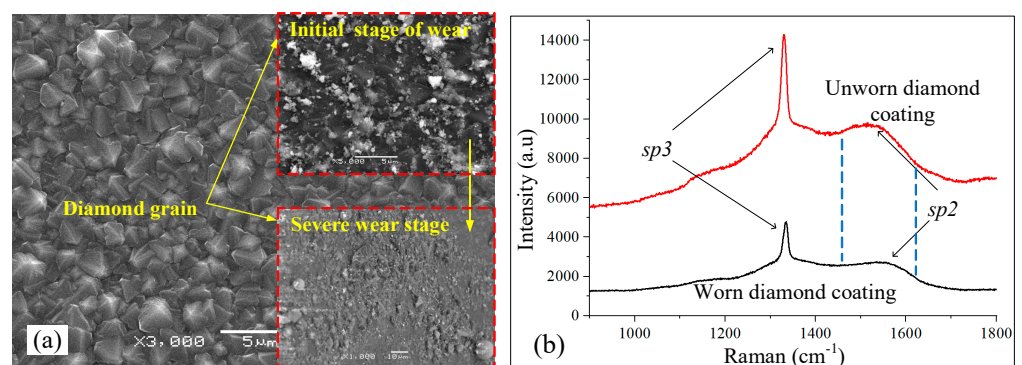


Figure 4. Wear and mechanism of Diamondcoated Tool. (a) Diamond coating wear (b) Raman spectra of worn and unworn diamond coatings.

3.2. The Mechanism of Action of Solid Lubricating Coatings

In the process of machining, there are three factors affecting the graphitization of diamonds coating, which are high temperature, Fe catalysis, and stress [31,32]. High temperature and intimate contact between diamond and iron not only transform diamond into graphite but also transform iron into a hexagonal structure. The transformation of bcc iron to hcp iron plays an important role in the graphitization of diamonds. This path is favorable energetically and geometrically for the subsequent diffusion of carbon into iron or the actual formation of a chemical reaction to form iron carbide (Fe_3C) [33]. WS_2 crystals were prepared in the vacuum environment, arranged in sheets, and perpendicular to the sample surface. Under the action of external force, WS_2 crystals are redirected. The crystals are transformed from a columnar arrangement to a layered structure, as shown in Figure 5. It not only blocks the contact between the chip and the blade surface but also reduces the shear stress and frictional heat of the coating. The layered structure with large surface energy is easily adsorbed on Fe chips to form agglomerates, which reduces the Fe content on the coating surface.

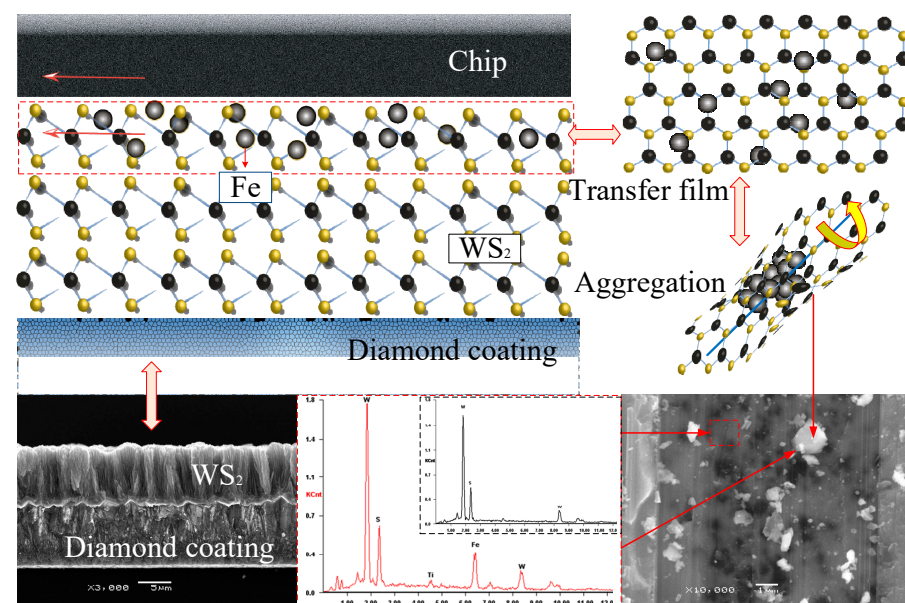


Figure 5. WS_2 inhibits the graphitization of diamonds.

The cutting lengths of the three cutting edges (A, B, C; I, II, III) are 50.2 m, 100.4 m, and 150.7 m, respectively. The cutting edge and rake face of CVD diamond-coated turning tools and WS_2/CVD diamond-coated turning tools have corresponding wear. With the increase in cutting distance, the cutting area is continuously affected by external stress and cutting heat. The cutting edge of the turning tool and the crater area of the rake face showed coating wear and delamination (Figure 6a), while the wear area of the WS_2/CVD Diamond-coated turning tool did not show delamination (Figure 6b). The CVD Diamond-coated turning tool appear a large area of delamination in the crater wear, while WS_2/CVD Diamond-coated turning tool only has local wear. It is proved that WS_2 coating is an effective means to restrain the wear and delamination of diamond coatings.

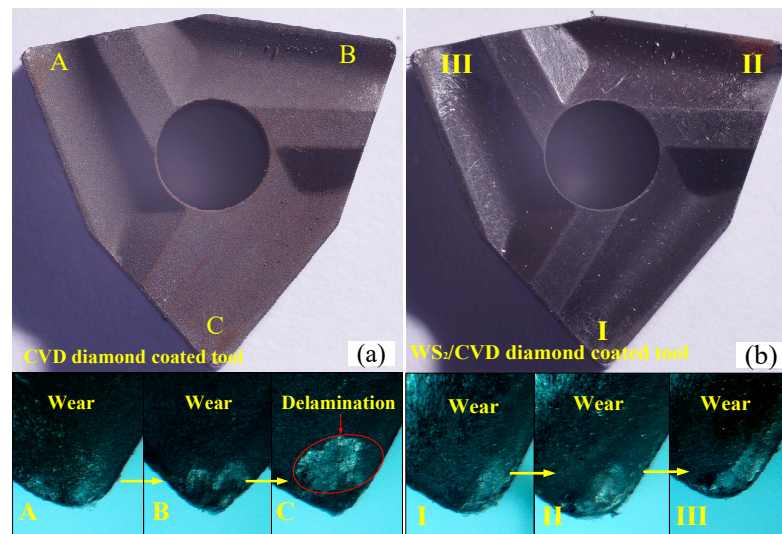


Figure 6. Wear and delamination of coatings. (a) CVD Diamond-coated tools (b) WS₂/CVD Diamond-coated tool. A/I: 50.2 m B/II: 100.4 m C/III: 150.7 m.

3.3. Effect of Micro-Textures on Adhesion Properties of Diamond Coatings

Micro-textures effectively improve the anti-wear and antifricition properties of the rake face and also affect the adhesion properties of the coating [34]. Displacement loading tests were conducted on textured and non-textured diamond-coated samples using an indentation testing machine. As shown in Figure 7a, uniform diamond coatings are prepared on textured cemented carbide by hot wire chemical vapor deposition (HFCVD). In order to explore the effect of micro-textures on the adhesion properties of diamond coatings, the Rockwell indentation tests were used to induce the delamination of the coating. Figure 7b shows the edge cracks of the indentation produced circumferential cracks, but radial cracks were rarely observed. Figure 7c,d show two types of crack propagation of texture edge coating. The indentation causes the diamond coating to peel off and expose the cemented carbide, a part of the circumferential crack bypasses the micro-textures, and the other part extends to the edge of the texture, causing fracture of the diamond coating.

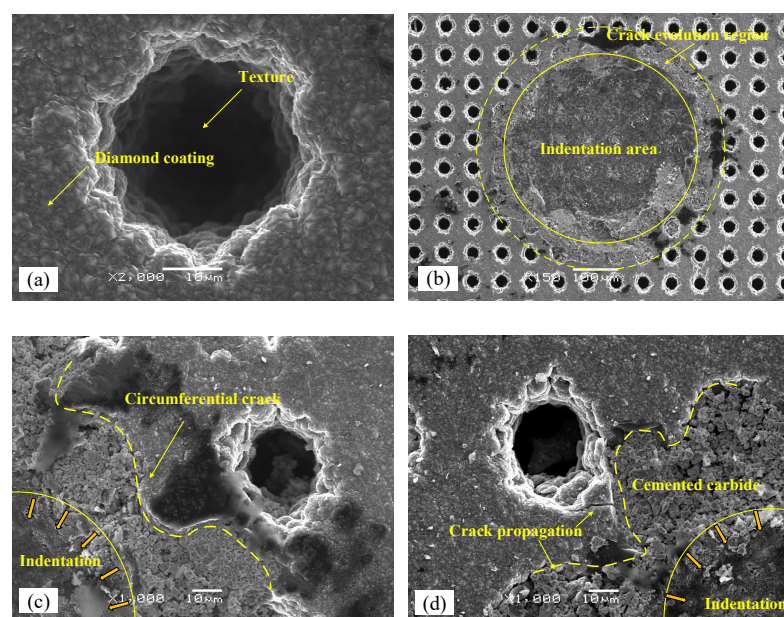


Figure 7. The indentation test causes the peeling of the textured coating. (a) Textured diamond coating. (b) Indentation. (c) Circumferential cracks. (d) Fracture of texture edge coating.

The crack propagation at the interface is the main reason for the delamination of the diamond coating, which makes the coating lose its bonding with the substrate, and the buckling phenomenon of the diamond coating occurs due to the action of intrinsic stress. As shown in Figure 8, the three-dimensional morphology of the indentation was observed by ultra-depth-of-field microscopy, and it was found that a higher bulge was generated around the indentation, which was due to the height difference caused by the buckling of the diamond coating. At the same load of 1471N, the indentation area of the textured coating-substrate system is larger, indicating that the texture reduces the strength of the substrate. However, it is observed that the buckling range of the textured diamond coating is smaller than that of the untextured coating from the contour plot. Obviously, micro-textures enhance the adhesion of the diamond coating.

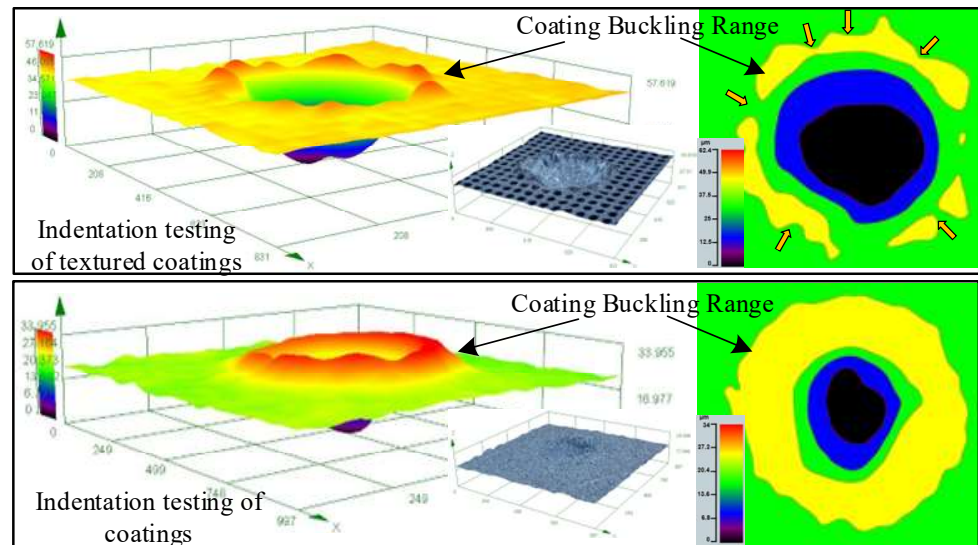


Figure 8. The three-dimensional shape of the indentations.

The effect of mechanical interlocking of micro-textures on coating-substrate adhesion is shown in Figure 9. Regardless of residual stresses and fracture of the coating, a stronger adhesion between the coating and the substrate occurs than that of the non-textured coating. Strong mechanical interlocking was formed between the membrane substrates. The texture density is $\pi r^2 / ab = \alpha$. If the toughness of the coating is high enough, the coating-substrate adhesion is only related to the texture profile and the shear and tensile strength of the interface, as shown in Equations (2)–(4).

$$\sigma_b ab = \sigma_b \pi r^2 / \alpha = F_i \tag{2}$$

$$(\tau_b \sin \theta + \sigma_b \cos \theta) \pi r^2 + \sigma_b (ab - \pi r^2) = F_j \tag{3}$$

$$\theta = \arctan f'(x) \tag{4}$$

where τ_b is the shear strength of the interface, σ_b is the tensile strength, θ is the angle between the tangent direction of the interface curve and the Y axis, $f(x)$ is the profile function, a is the length, r is the texture radius, and F_i is Textured coating adhesion, F is the non-textured coating adhesion.

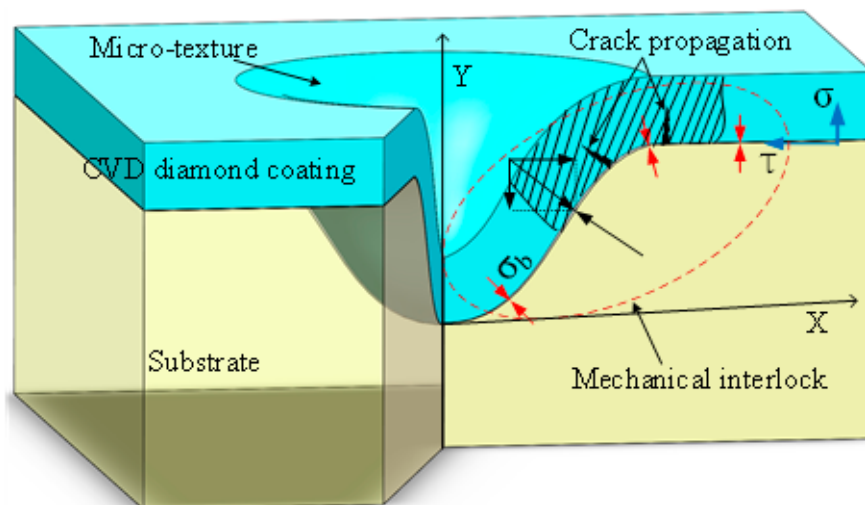


Figure 9. Micro-textured coating-substrate mechanical interlocking.

However, as shown in Figure 7, the fracture of the coating at the edge of the textures indicates that the toughness of the coating affects the coating-substrate mechanical interlocking of the texture. Therefore, the model considering coating fracture is more reasonable. The fracture of the microtextured edge diamond coating exists in two forms: cracks perpendicular to the interface and cracks parallel to the interface. The shear strength, fracture strength, thickness of diamond coating and the size of micro-textures affect the mechanical properties of the coating-substrate system. The shear force and normal force that the textured diamond coating could bear are shown in Equation (5). The fracture position of textured coating can be determined by the formula.

$$\begin{cases} F_i = S\sigma_i \\ F_{\sigma_i} = S_1\sigma_d + S_2\sigma_i \\ F_{\sigma_j} = S_3\tau_d + S_2\sigma_i \end{cases} \quad (5)$$

where σ_d is the tensile strength of the interface, τ_d is the shear strength of the interface, a and b are the side lengths, and σ and τ are the tensile strength and shear strength of the diamond coating, respectively. S_1 is the parallel fracture area, S_2 is the interface fracture area, and S_3 is the vertical fracture area. Their calculation formulas are: $S_1 = \pi[r^2 - (r - h)^2]$, $S_2 = \pi r^2(1/\alpha - 1)$, $S_3 = 2\pi rh$.

Micro-textures produce a mechanical interlocking effect between coating and substrate, which produce the coating adhesion are increased to a certain extent. However, the selection of micro-texture size is very critical. It is mentioned in the relevant literature that the above normal bond force is 200 MPa, and the tensile strength and shear strength of CVD diamond coating are 580 MPa and 348 MPa [35]. The calculated area is assumed to be 0.1×0.1 mm, and the radius of the texture and the thickness of the coating are variables. As shown in Figure 10, F_{σ_i} represents the force required for the coating to peel off when the fracture occurs parallel to the interface. F_{σ_j} represents the force required for the coating to peel off when the fracture position occurs perpendicular to the interface. As the thickness of the diamond coating increases, the normal delamination force of the diamond coating shows an obvious upward trend. When the texture radius is small, and the coating thickness is large, the curved surfaces of the two forces intersect, forming a demarcation line, and the position of the fracture becomes parallel to the interface. Compared with the untextured samples, the effect of texture on improving the adhesion of coating is very obvious.

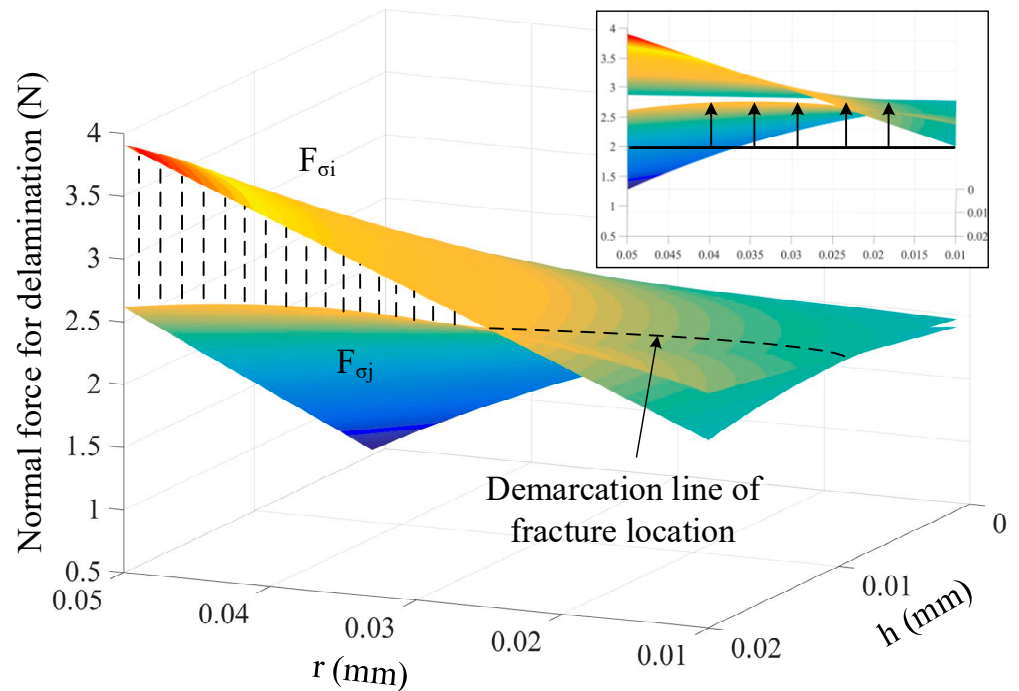


Figure 10. Variation of delamination force.

Under the premise of considering the fracture of diamond coating, the fracture strength and coating thickness of the diamond coating has a significant effect on the normal delamination force of the textured diamond coating. The adhesion of diamond coating can be greatly improved by increasing the toughness of the coating and choosing the appropriate texture size and thickness of the coating.

3.4. Effect of Micro-Textures on Residual Stress of Diamond Coating

In addition, due to the particularity of the CVD process, the residual stress generated inside the coating-substrate system and micro-textures affect the stress state of the coating. The stress distribution characteristics of the texture edge were analyzed by thermal-structure coupling simulation, as shown in Figure 11. There is a stress concentration at the edge of the texture. Excessive stress greatly promotes the propagation of cracks inside the diamond coating, and the large difference between the stress in the coating and substrate also results in the propagation of interfacial cracks. In coating-substrate systems, normal stress is the main cause of opening-type cracks (Type I). It can be observed in Figure 11b that there is normal compressive stress in the coating inside the micro-texture, which undoubtedly strengthens the coating-substrate mechanical interlocking effect of the micro-texture. At the texture edge, there is tensile stress inside the substrate, so the toughness of the substrate has a significant effect on the adhesion of the coating-substrate system. During the cooling process of the coating-substrate system, the shear stress of the coating exhibits symmetry, as shown in Figure 11c, and the stress state inside the coating is opposite to that of the substrate. In order to explore the variation law of stress near the interface, a line segment is inserted at the interface near the texture edge, and it is found that the equivalent stress of the texture edge is larger, and the minimum stress exists in the region near the texture edge. The stress state at the coating-substrate interface inside the texture is compressive stress, which gradually transforms into tensile stress as the distance increases.

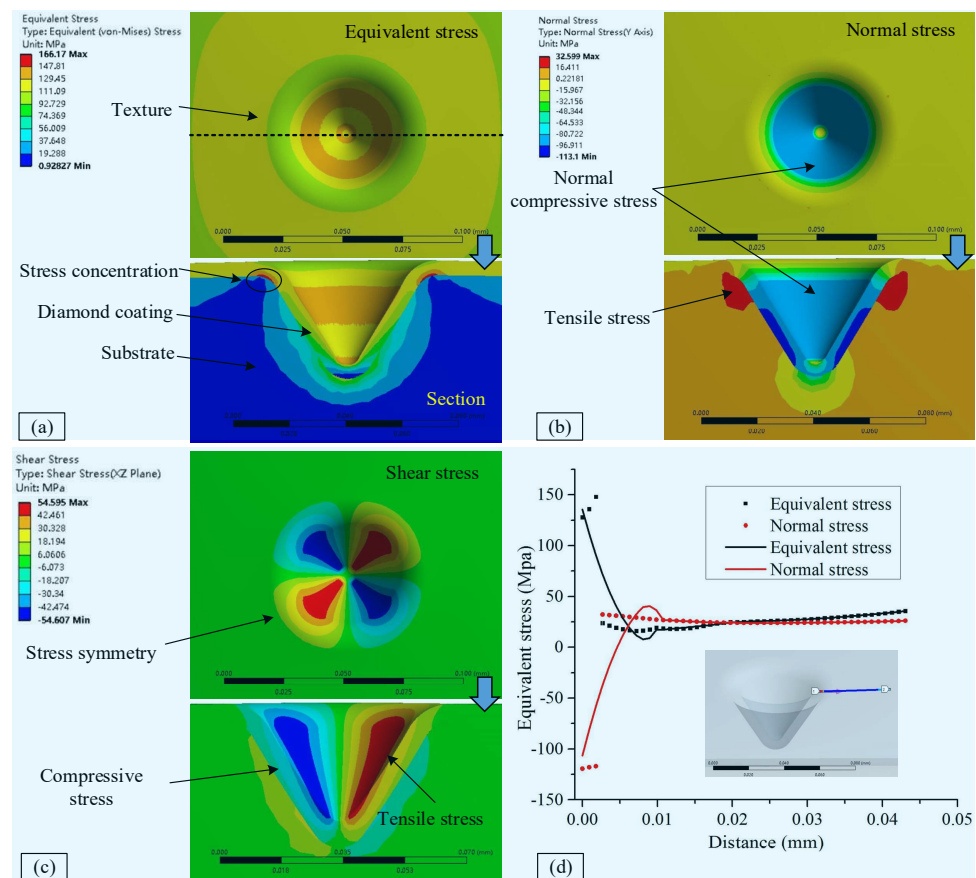


Figure 11. The effect of texture on stress. (a) Equivalent stress (b) Normal stress (c) Shear stress (d) The change of texture edge stress.

In conclusion, the microtextures suppressed the propagation of interfacial cracks and enhanced the adhesion properties of the coatings. Without considering the residual stress, the mechanical interlocking effect of the coating-substrate produced by the texture is the main reason that affects the adhesion performance. The fracture strength, coating thickness, radius, and area ratio of micro-textures of the coating significantly affect the delamination force of the coating. In addition, the existence of micro-texture also affects the residual stress of diamond coating, which puts forward higher requirements on the toughness of diamond coating and substrate. The high toughness of diamond coating and substrate becomes the premise of forming the coating-substrate mechanical interlocking.

4. Study on Cutting Performance of Textured Diamond-coated Cutting Tools

4.1. Textured Diamond-Coated Tools

Micro-textures were fabricated at the rake face by UV nanosecond laser, diamond coatings, and WS_2 coatings were deposited by HFCVD and RF magnetron sputtering technology, as shown in Figure 12.

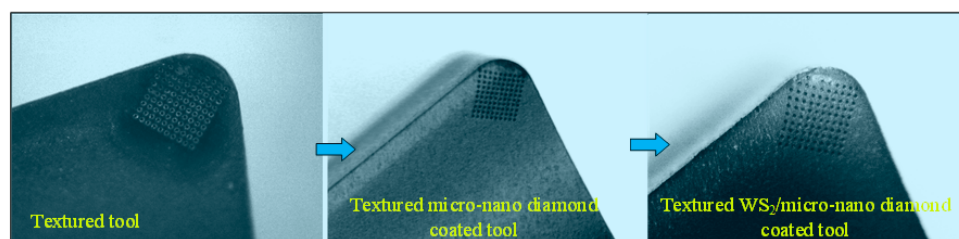


Figure 12. Preparation of textured micro-nano Diamond-coated cutting tool.

It is worth noting that the form of our diamond coating is micron diamond coating as the main body, and there is a thin nano diamond coating at the top (Figure 13), which is conducive to reducing the micro-cutting effect of micron crystal formation and forming space for storing solid lubricating coating, and is beneficial to reduce external stress [36], and the reduction in external stress is conducive to less delamination probability, as shown in Equation (1). The grain size is controlled by the methane content of the gas source and the pressure in the chamber. The key to depositing nanocrystalline diamond coating is to improve the secondary nucleation rate of the diamond coating. From a nanoscale thermodynamic point of view, the nucleation of CVD diamond takes place in the stable region of the carbon thermodynamic equilibrium phase diagram; in the competitive growth with graphite, due to the additional pressure induced by the curvature of the nanocrystalline surface, the diamond shape nuclei are formed prior to graphite, and the role of hydrogen atoms is to etch the graphitic phase and promote the sp^3 hybridization of carbon. Increasing the carbon source concentration can increase the nucleation density and secondary nucleation rate.

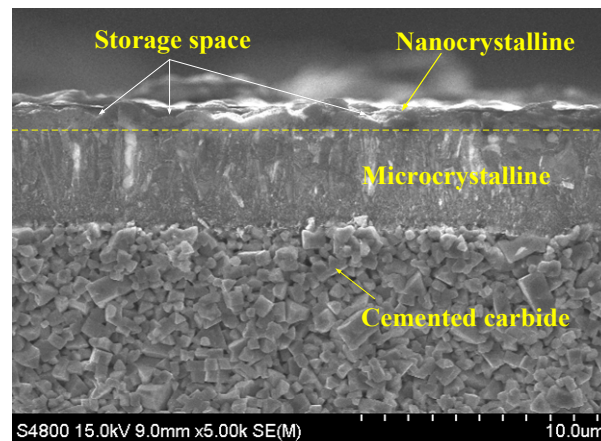


Figure 13. Micro-nanocrystalline diamond coating.

As shown in Figure 14a, WS_2 and diamond coatings of the same thickness are deposited, and there is a transition layer W between them. The crystals of WS_2 form a sheet structure and grow perpendicular to the interface. The bonding force between the sheets is small, leading to the evolution of cracks in the coating (Figure 14b). The lamellar crystal structure and the small van der Waals forces between the crystals are the basis for the lubrication of the coating.

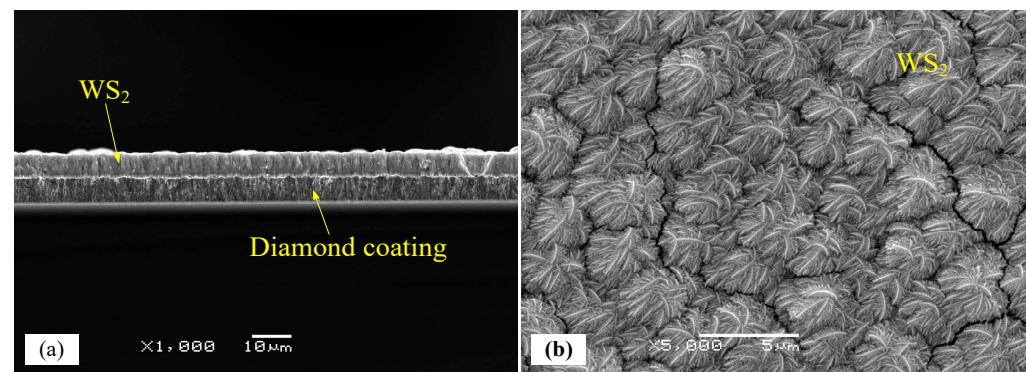


Figure 14. Soft and hard composite coating. (a) Deposition of WS_2 on diamond coating (b) WS_2 coating.

4.2. Anti-Delamination and Anti-Wear of Textured Diamond-Coated Cutting Tools

W/MNDCT and T-W/MNDCT exhibited distinct wear states at the same cutting parameters and cutting distance, as shown in Figure 15. The most severely worn area is the crater area, where the cutting temperature is the highest, accompanied by huge positive compressive stress and shear stress. In the worn area, the micrograins that are worn into planes can be clearly observed (Figure 15a). As the WS₂ coating and surface nanocrystals wear away, the microcrystals gradually participate in the friction process at the tool-chip interface. A stagnant layer appears in the local area of the rake face of the tool, as shown in Figure 15b. Once the coating was worn through, delamination of the diamond coating appeared immediately due to the direct exposure of the coating-substrate interface to the action of cutting chips (Figure 15c,d). Obviously, the coating delamination of diamond-coated tools with textures on the rake face is effectively suppressed. As shown in Figure 15e–h, the loss of WS₂ and the wear of the diamond coating also appear on the rake face, but there was no delamination of the coating. The main reason lies in the capture and reuse of WS₂ transfer film by micro-textures and the interlocking effect of coating substrate generated by micro-textures. Therefore, the micro-textures effectively enhance the coating adhesion, but the micro-textures near the cutting edge produce secondary shear and increase the cutting force, so the position design of the texture is also particularly important. Figure 15d,h show different states on the rake face of the tool under the same cutting amount and cutting time. The rake face of the non-textured tool has a large area of coating peeling off, while the surface of the textured tool has no obvious coating peeling. This proves that micro-texture plays an important role in inhibiting coating peeling and wear.

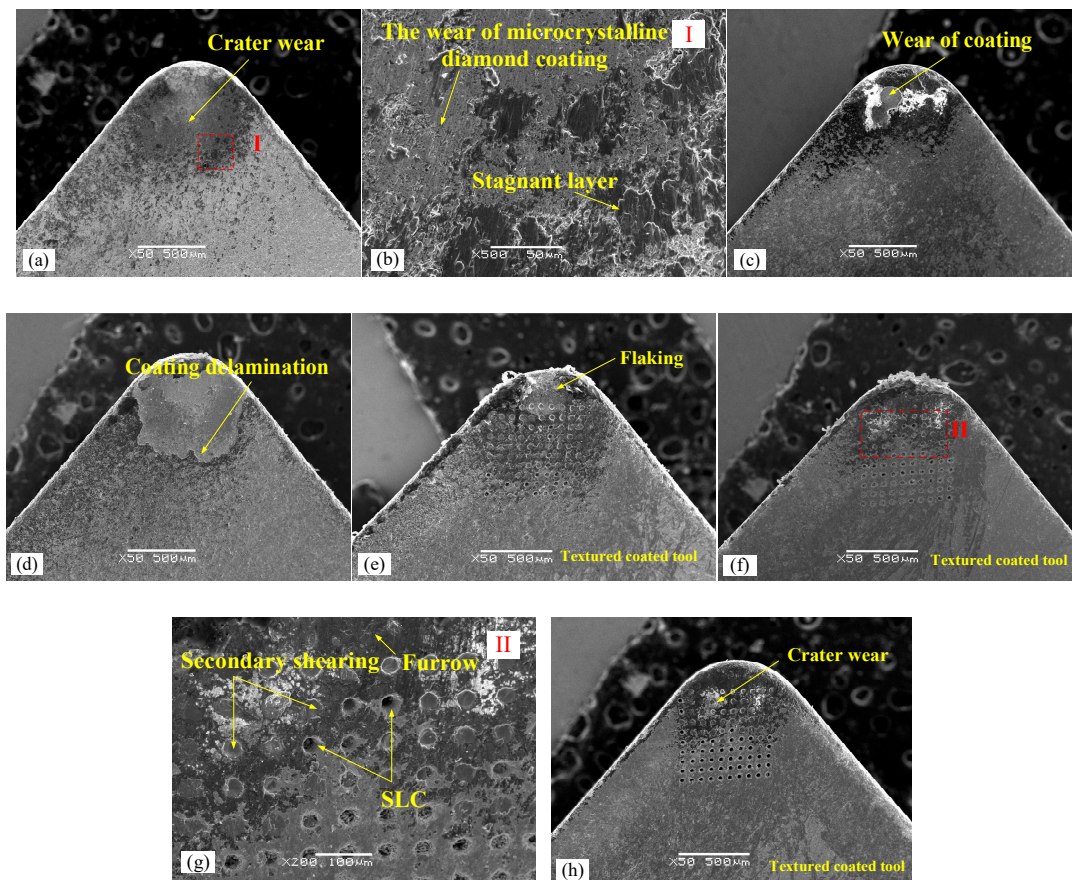


Figure 15. Wear and peeling of WS₂/diamond coatings. (a) Initial wear stage (b) Crater wear (c) Coating worn through by chip (d) Coating delamination (e) Initial wear stage of textured tool (f) Coating wear (g) Crater wear of textured tool (h) Final wear pattern.

In order to further reduce the external stress (σ_e) on the coating, reduce the friction coefficient at the interface, and at the same time ensure sufficient storage of WS_2 in the intergranular space, a thin nanocrystalline diamond coating was proposed to cover the microcrystalline diamond coating. The method, on the one hand, increases the contact radius of the diamond coating grain tip and reduces the interface shearing action. On the other hand, a larger surface roughness is obtained, which is beneficial for storing WS_2 and suppresses the loss of WS_2 . In the cutting process of diamond-coated tools, the micro-crystals increase the micro-cutting force between chips, workpieces, and coating. On the other hand, it could increase the external stress on the coating (Figure 16). Growing a thin layer of nanocrystalline diamond coating on the microcrystalline diamond coating can not only avoid too-sharp diamond exposure but also copy the surface morphology of the microcrystalline to form wave peaks and troughs, which are used to store solid lubricating coatings.

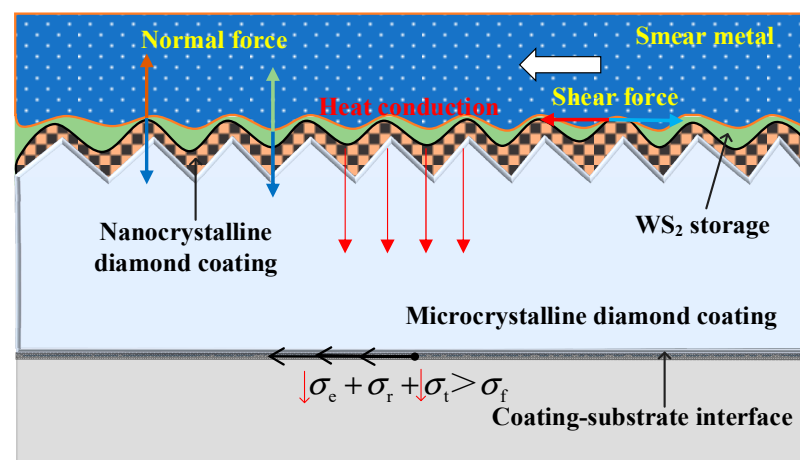


Figure 16. Mechanism of micro-nanocrystalline coating inhibiting coating peeling.

In order to understand the coating wear process of the rake face more clearly, the representative wear topography characteristics were observed and discussed. The synergistic effect of WS_2 coating and micro/nanodiamond coating is the key to achieving friction reduction and wear resistance on the tool front surface. The movement and distribution of material on the knife-chip contact area can be understood through the morphology of the tool front surface, and the principle of friction reduction and wear resistance can be further understood. The nanocrystals of the diamond coating are in the shape of a cauliflower, and the existence of the base microcrystals leads to the undulating shape of the nanocrystal coating as a whole, which with many peaks and troughs (Figure 17a). In the initial stage of the tool-cutting process, the micro-texture captures the transfer film to form a storage of solid lubricant, and the surface of the diamond coating is covered by WS_2 to realize the lubrication of the tool (Figure 17b). Figure 17c–e reveals the wear process on the tool surface. With the flow of chips, WS_2 is lost due to its own transfer film mechanism. In contrast, the cauliflower-like diamond grains penetrate the WS_2 coating and bear part of the normal load, which inhibit the loss of the WS_2 coating. As the WS_2 is depleted, the nanocrystalline diamond coating gradually participates in interfacial friction. After the nanocrystalline diamond coating wears, the SLC stored in the valley gradually participates in friction. When the cauliflower particles are worn, the microcrystalline diamond coating, nanodiamond coating, and SLC coexist at the friction interface. The WS_2 coating in the grain gap participates in the friction process and minimizes the sticking phenomenon. Therefore, the textured WS_2 /micro-nano diamond coating tool not only own the synergistic friction-reducing effect of the microtextures-SLC but also has the effect of the nanodiamond coating to inhibit the loss of WS_2 , which improves the self-lubricating properties of the tools. Figure 17f–i show the EBS images at the later stage of wear, observing the elemental

distribution on the surface. Most of the micro-textures produced secondary shearing, and a large amount of iron was stored inside the textures. There is a white reflective area in Figure 17g, and EBS shows that there are a large number of carbon atoms in this area, but there is no W atom (Figure 17h,i), which proves that the WC on the tool substrate is not exposed, and there is a diamond coating on the surface.

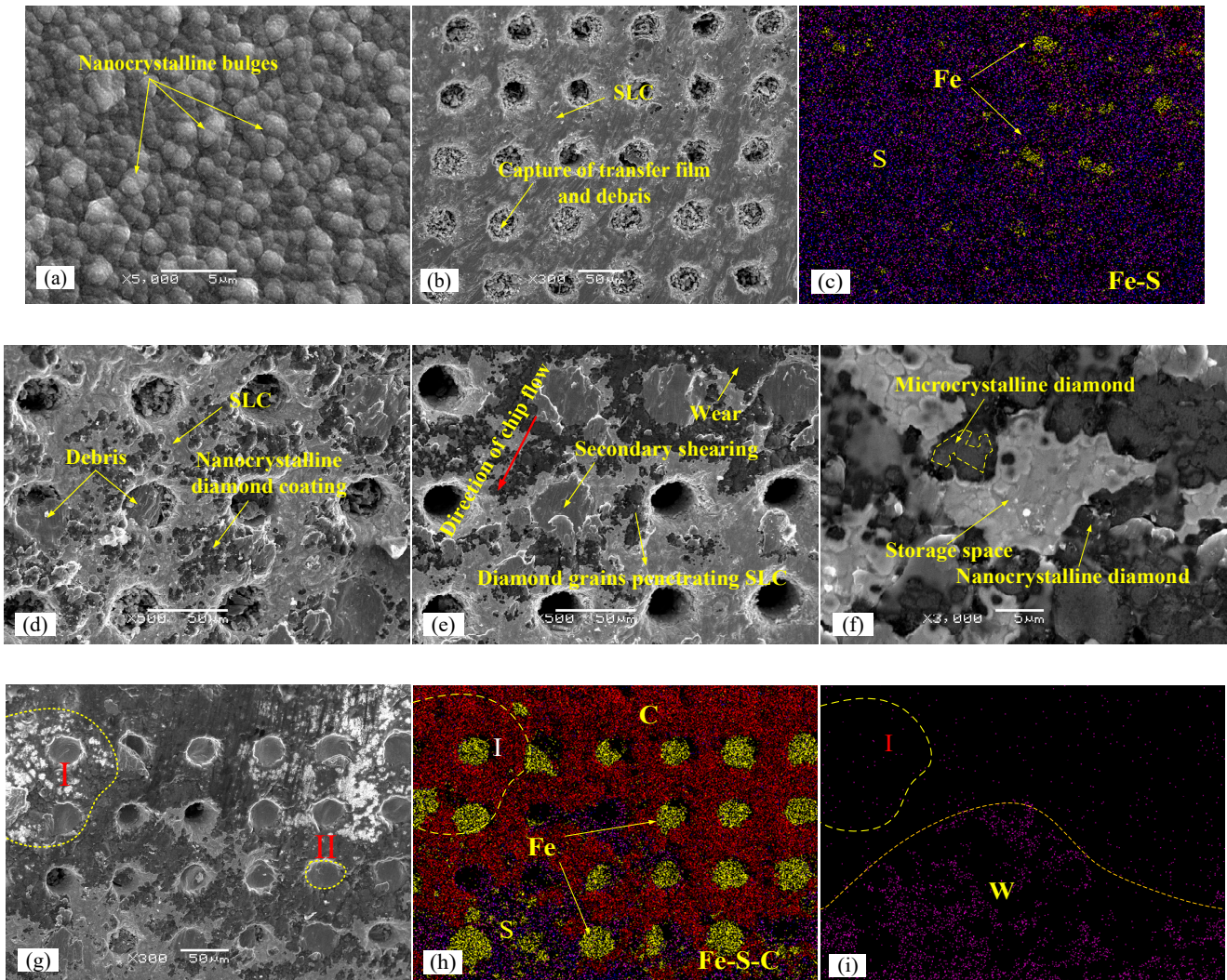


Figure 17. Micro-morphology of rake face. (a) Nanocrystal diamond coating (b) Initial wear (c) Distribution of Fe and S elements (d) Nanodiamonds exposed after WS_2 loss (e) Secondary shearing (f) Storage area of solid lubricant (g) Crater wear (h) Distribution of Fe and C elements (i) Distribution of W element.

4.3. Element Change and Oxidation of WS_2 on the Rake Face

Figure 18a,b show the comparison of element distribution in the early and late stages of wear in the tool crescent area, respectively. The detection of crescent craters shows that W and S elements are decreasing and Fe elements are increasing, which is caused by the loss of WS_2 and secondary shear. It is worth noting that there are more W elements than S. On the one hand, W has a stronger response to the energy spectrum, and on the other hand, WS_2 decomposes and oxidizes at high temperatures, and the distribution of O elements verifies this conclusion. The diamond coating is exposed after WS_2 depletion, leading to a sharp increase in the detected C element content.

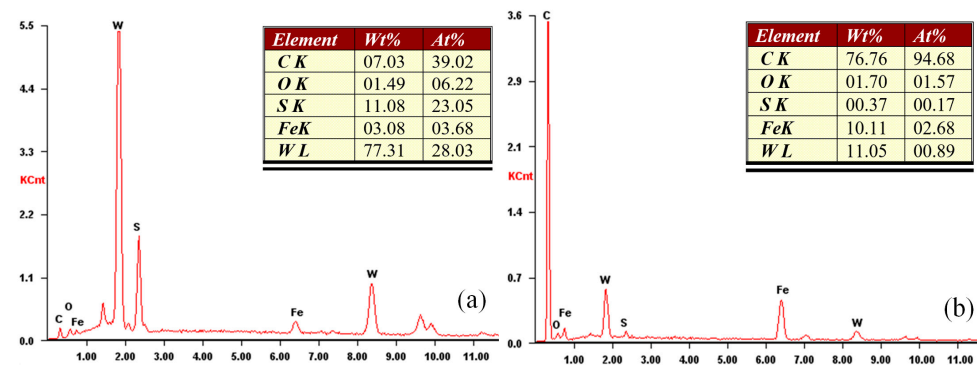


Figure 18. Element distribution of crater. (a) Element distribution in the early stage (b) Element distribution in the late stage.

The full width at half maximum (FWHM) of the sp^3 carbon peak of the micro-nano composite diamond coating is significantly different from that of the microcrystalline diamond coating. The broadening of the sp^3 carbon peak FWHM and the decrease in the crystallinity of diamond (the increase in defects and nonlinearity) have a direct relationship, and the broadening of the diamond peak is also related to the content of sp^2 carbon [37]. Figure 19 shows that the ratio of the sp^2 carbon peak to the sp^3 carbon peak (I_n/I_{diamond}) increased after the cutting test, proving that the graphitization of diamonds occurred during the cutting process, which was related to the high temperature, oxidation reaction and the reaction between Fe and C under cutting conditions. The Raman spectrum of the solid lubricating coating in the interstices of the cauliflower-like nanodiamond grains has obvious characteristic peaks of WS_2 , WO_3 , and graphite, which proves that the solid lubricating coating in the interstices is a mixture of WS_2 , WO_3 , and graphite. The oxidation reaction of WS_2 produces WO_3 , which also has a certain lubricating effect under high-temperature conditions. The diamond grains generate graphite at the interface, and the graphite transfers into the grain gap and continues to participate in the interface friction, increasing the lubricating performance of the tool-chip interface.

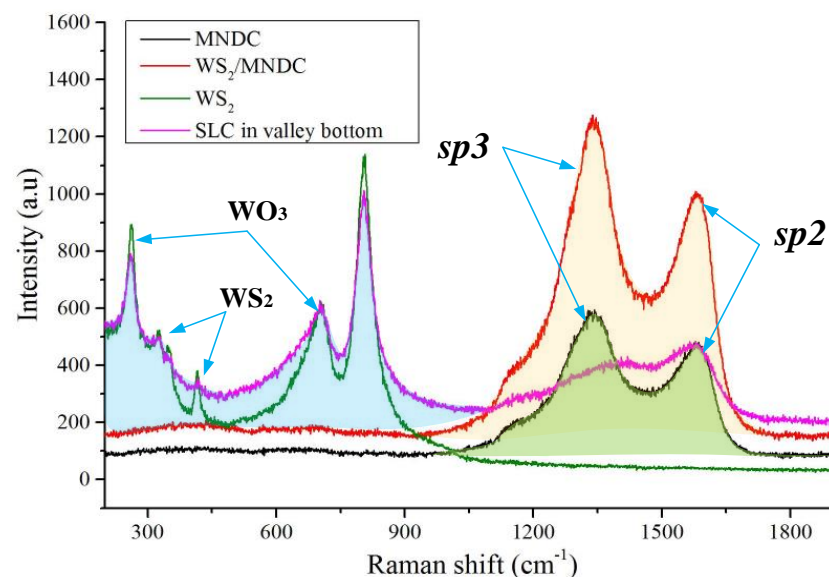


Figure 19. Raman spectrum of rake face coating.

5. Conclusions

The purpose of this study is to address the challenges associated with the delamination of diamond coatings and tool wear while avoiding issues of diamond coating fracture and peeling caused by liquid lubrication and cooling-induced temperature reduction. It is

especially suitable for use in situations where severe friction occurs. The key findings of this research are summarized as follows.

- 1 WS_2 forms agglomerates that enclose iron debris at the interface of the abrasive pair, resulting in a reduction in iron content at the interface and effectively preventing the graphitization of the diamond coating.
- 2 Microtexturing enhances the adhesion performance of the diamond coating; however, stress concentration is observed at the edges of the texture.
- 3 The combination of microtexturing with WS_2 in the micro/nanodiamond coatings acts as a reservoir for WS_2 .
- 4 The textured WS_2 /micro-nanodiamond-coated cutting tools have demonstrated excellent wear and peel resistance, with a wear resistance performance exceeding that of diamond-coated cutting tools by more than three times.

Author Contributions: Z.Z.: Methodology, Experiment, Data curation, Writing—original draft. X.Q.: Experiment, Writing—review & editing. S.M.: Conceptualization, Supervision. Y.L.: Validation. L.W.: Investigation, Simulation. X.Z.: Simulation, Writing—review & editing. All authors have read and agreed to the published version of the manuscript.

Funding: This project is supported by the Science Fund of Shandong Laboratory of Advance Materials and Green Manufacturing (Yantai) (AMGM2023F01) and the Science Fund of Jiangsu Provincial Key Laboratory of Precision and Micro Manufacturing Technology (JX23KH008).

Data Availability Statement: Data available on request from the authors.

Conflicts of Interest: The authors declare no conflict of interest.

References

1. Ramasubramanian, K.; Arunachalam, N.; Rao, M.R. Wear performance of nano-engineered boron doped graded layer CVD diamond coated cutting tool for machining of Al-SiC MMC. *Wear* **2019**, *426–427*, 1536–1547. [[CrossRef](#)]
2. Zhuang, G.; Zong, W.; Tang, Y.; Cui, Z. Crystal orientation and material type related suppression to the graphitization wear of micro diamond tool. *Diam. Relat. Mater.* **2022**, *127*, 109182. [[CrossRef](#)]
3. Xu, J.; Ji, M.; Davim, J.P.; Chen, M.; El Mansori, M.; Krishnaraj, V. Comparative study of minimum quantity lubrication and dry drilling of CFRP/titanium stacks using TiAlN and diamond coated drills. *Compos. Struct.* **2019**, *234*, 111727. [[CrossRef](#)]
4. Jiang, G.; Jianguo, Z.; Yanan, P.; Renke, K.; Yoshiharu, N.; Paul, S.; Xiaobin, Y.; Baorui, W.; Dongming, G. A critical review on the chemical wear and wear suppression of diamond tools in diamond cutting of ferrous metals. *Int. J. Extrem. Manuf.* **2019**, *2*, 012001. [[CrossRef](#)]
5. Zou, L.; Yin, J.; Huang, Y.; Zhou, M. Essential causes for tool wear of single crystal diamond in ultra-precision cutting of ferrous metals. *Diam. Relat. Mater.* **2018**, *86*, 29–40. [[CrossRef](#)]
6. Bulla, B.; Klocke, F.; Dambon, O.; Hüntten, M. Influence of Different Steel Alloys on the Machining Results in Ultrasonic Assisted Diamond Turning. *Key Eng. Mater.* **2012**, *523–524*, 203–208. [[CrossRef](#)]
7. Tang, Q.; Yin, S.; Chen, F.; Huang, S.; Luo, H. New technology for cutting ferrous metal with diamond tools. *Diam. Relat. Mater.* **2018**, *88*, 32–42. [[CrossRef](#)]
8. Feng, J.; Qin, Y.; Liskiewicz, T.W.; Beake, B.D.; Wang, S. Crack propagation of a thin hard coating under cyclic loading: Irreversible cohesive zone model. *Surf. Coat. Technol.* **2021**, *426*, 127776. [[CrossRef](#)]
9. Ma, D.-D.; Xue, Y.-P.; Gao, J.; Ma, Y.; Yu, S.-W.; Wang, Y.-S.; Xue, C.; Hei, H.-J.; Tang, B. Effect of Ta diffusion layer on the adhesion properties of diamond coating on WC-Co substrate. *Appl. Surf. Sci.* **2020**, *527*, 146727. [[CrossRef](#)]
10. Brinksmeier, E.; Gläbe, R.; Osmer, J. Diamond Cutting of FeN-Layers on Steel Substrates for Optical Mould Making. *Key Eng. Mater.* **2010**, *438*, 31–34. [[CrossRef](#)]
11. Zou, L.; Huang, Y.; Zhou, M.; Yang, Y. Effect of cryogenic minimum quantity lubrication on machinability of diamond tool in ultraprecision turning of 3Cr₂NiMo steel. *Mater. Manuf. Process.* **2017**, *33*, 943–949. [[CrossRef](#)]
12. Bounif, K.; Abbadi, M.; Atlati, S.; Nouari, M.; Selvam, R. Modeling and Numerical Simulation of the Cracking of a Diamond-Coated Cutting Tool during Machining. *Key Eng. Mater.* **2019**, *820*, 29–39. [[CrossRef](#)]
13. Chai, H. Multi-crack analysis of hydraulically pumped cone fracture in brittle solids under cyclic spherical contact. *Int. J. Fract.* **2007**, *143*, 1–14. [[CrossRef](#)]
14. Lian, Y.; Chen, H.; Mu, C.; Deng, J.; Lei, S. Experimental Investigation and Mechanism Analysis of Tungsten Disulfide Soft Coated Micro-Nano Textured Self-Lubricating Dry Cutting Tools. *Int. J. Precis. Eng. Manuf. Technol.* **2018**, *5*, 219–230. [[CrossRef](#)]
15. Suarez, M.P.; Marques, A.; Boing, D.; Amorim, F.L.; Machado, Á.R. MoS₂ solid lubricant application in turning of AISI D6 hardened steel with PCBN tools. *J. Manuf. Process.* **2019**, *47*, 337–346. [[CrossRef](#)]

16. Rosenkranz, A.; Costa, H.L.; Baykara, M.Z.; Martini, A. Synergetic effects of surface texturing and solid lubricants to tailor friction and wear—A review. *Tribol. Int.* **2020**, *155*, 106792. [[CrossRef](#)]
17. Li, C.; Duan, L.; Tan, S.; Zhang, W.; Pan, B.; Chikhotkin, V. Study on the effectiveness of WS₂ and CaF₂ on the performances of self-lubricating micro impregnated diamond bits. *Int. J. Refract. Met. Hard Mater.* **2019**, *84*, 105021. [[CrossRef](#)]
18. Lu, Z.; Zhang, C.; Zeng, C.; Ren, S.; Pu, J. A novel design by constructing MoS₂/WS₂ multilayer film doped with tantalum toward superior friction performance in multiple environment. *J. Mater. Sci.* **2021**, *56*, 17615–17631. [[CrossRef](#)]
19. Zhang, Z.; Feng, W.; Lu, W.; Du, X. Preparation and tribological properties of micro-textured diamond/WS_x coatings. *Surf. Coat. Technol.* **2020**, *403*, 126369. [[CrossRef](#)]
20. Gajrani, K.K.; Sankar, M.R.; Dixit, U.S. Environmentally friendly machining with MoS₂-filled mechanically microtextured cutting tools. *J. Mech. Sci. Technol.* **2018**, *32*, 3797–3805. [[CrossRef](#)]
21. Xing, Y.; Deng, J.; Wu, Z.; Liu, L.; Huang, P.; Jiao, A. Analysis of tool-chip interface characteristics of self-lubricating tools with nanotextures and WS₂/Zr coatings in dry cutting. *Int. J. Adv. Manuf. Technol.* **2018**, *97*, 1637–1647. [[CrossRef](#)]
22. Zheng, K.; Gao, J.; Hei, H.; Wang, Y.; Yu, S.; He, Z.; Tang, B.; Wu, Y. Design and fabrication of HfC, SiC/HfC and HfC-SiC/HfC interlayers for improving the adhesion between diamond coatings and cemented carbides. *J. Alloys Compd.* **2020**, *815*, 152405. [[CrossRef](#)]
23. Xiang, D.; Su, Z.; Li, Y.; Zhang, Z. The effect of laser texture on adhesion and tribological properties of boron-doped diamond film on WC-Co cemented carbide. *Diam. Relat. Mater.* **2022**, *130*, 109469. [[CrossRef](#)]
24. Zhang, Z.; Lu, W.; Feng, W.; Du, X.; Zuo, D. Effect of substrate surface texture on adhesion performance of diamond coating. *Int. J. Refract. Met. Hard Mater.* **2021**, *95*, 105402. [[CrossRef](#)]
25. Zhang, K.; Deng, J.; Ding, Z.; Guo, X.; Sun, L. Improving dry machining performance of TiAlN hard-coated tools through combined technology of femtosecond laser-textures and WS₂ soft-coatings. *J. Manuf. Process.* **2017**, *30*, 492–501. [[CrossRef](#)]
26. Meng, X.; Zhang, K.; Guo, X.; Wang, C.; Sun, L. Preparation of micro-textures on cemented carbide substrate surface by plasma-assisted laser machining to enhance the PVD tool coatings adhesion. *J. Mater. Process. Technol.* **2021**, *288*, 116870. [[CrossRef](#)]
27. Sojková, M.; Sifalovic, P.; Babchenko, O.; GabrielVanko; Dobročka, E.; Hagara, J.; Mrkyvkova, N.; Majková, E.; Ižák, T.; Kromka, A. Carbide-free one-zone sulfurization method grows thin MoS₂ layers on polycrystalline CVD diamond. *Sci. Rep.* **2019**, *9*, 2001. [[CrossRef](#)]
28. Damm, D.D.; Cardoso, A.C.L.D.R.; Trava-Airoldi, V.J.; Barquete, D.M.; Corat, E.J. A novel method to mitigate residual stress in CVD diamond film on steel substrates with a single intermediate layer. *Surf. Coat. Technol.* **2019**, *357*, 93–102. [[CrossRef](#)]
29. Hua, C.; Yan, X.; Wei, J.; Guo, J.; Liu, J.; Chen, L.; Hei, L.; Li, C. Intrinsic stress evolution during different growth stages of diamond film. *Diam. Relat. Mater.* **2019**, *73*, 62–66. [[CrossRef](#)]
30. Paprocki, K.; Dittmar-Wituski, A.; Trzciński, M.; Szybowicz, M.; Fabisiak, K.; Dychalska, A. The comparative studies of HFCVD diamond films by Raman and XPS spectroscopies. *Opt. Mater.* **2019**, *95*, 109251. [[CrossRef](#)]
31. Gogotsi, Y.G.; Kailer, A.; Nickel, K.G. Transformation of Diamond to Graphite. *Nature* **1999**, *401*, 663–664. [[CrossRef](#)]
32. Nechaev, D.V.; Khokhryakov, A.F. Formation of epigenetic graphite inclusions in diamond crystals: Experimental data. *Russ. Geol. Geophys.* **2013**, *54*, 399–405. [[CrossRef](#)]
33. Narulkar, R. Investigation on the Mechanism of Wear of Single Crystal Diamond Tool in Nanometric Cutting of Iron Using Molecular Dynamics (MD) and the Development of Generalized Potential Energy Surfaces (GPES) Based on Ab Initio Calculations. Ph.D. Thesis, Oklahoma State University, Stillwater, OK, USA, 2009.
34. Wang, J.; Bai, X.; Shen, X.; Liu, X.; Wang, B. Effect of micro-texture on substrate surface on adhesion performance of electroless Ni-P coating. *J. Manuf. Process.* **2022**, *74*, 296–307. [[CrossRef](#)]
35. An, K.; Li, S.; Shao, S.; Liu, P.; Liu, J.; Chen, L.; Wei, J.; Zheng, Y.; Liu, Q.; Li, C. Evaluation of the fracture strength of ultra-thick diamond plate by the three-point bending ISO standard method. *Ceram. Int.* **2022**, *48*, 17942–17949. [[CrossRef](#)]
36. Tan, N.; Xing, Z.-G.; Wang, X.-L.; Wang, H.-D.; Jin, G.; Xu, B.-S. Effects of texturing patterns on the adhesion strength of atmosphere plasma sprayed coatings. *J. Mater. Res.* **2017**, *32*, 1682–1692. [[CrossRef](#)]
37. Shimada, S.; Tanaka, H.; Higuchi, M.; Yamaguchi, T.; Honda, S.; Obata, K. Thermo-Chemical Wear Mechanism of Diamond Tool in Machining of Ferrous Metals. *CIRP Ann. -Manuf. Technol.* **2004**, *53*, 57–60. [[CrossRef](#)]

Disclaimer/Publisher's Note: The statements, opinions and data contained in all publications are solely those of the individual author(s) and contributor(s) and not of MDPI and/or the editor(s). MDPI and/or the editor(s) disclaim responsibility for any injury to people or property resulting from any ideas, methods, instructions or products referred to in the content.